



Article

Screen-Printed Electrode Surface Modification with NiCo₂O₄/RGO Nanocomposite for Hydroxylamine Detection

Somayeh Tajik ¹, Hadi Beitollahi ^{2,*}, Sayed ali Ahmadi ³ , Mohammad Bagher Askari ⁴
and Antonio Di Bartolomeo ^{5,*}

¹ Research Center of Tropical and Infectious Diseases, Kerman University of Medical Sciences, Kerman P.O. Box 76169-13555, Iran; s.tajik@kmu.ac.ir

² Environment Department, Institute of Science and High Technology and Environmental Sciences, Graduate University of Advanced Technology, Kerman P.O. Box 76318-85356, Iran

³ Department of Chemistry, Kerman Branch, Islamic Azad University, Kerman P.O. Box 76351-31167, Iran; saahmadi@iauk.ac.ir

⁴ Department of Physics, Faculty of Science, University of Guilan, Rasht P.O. Box 41335-1914, Iran; mbaskari@phd.guilan.ac.ir

⁵ Department of Physics "E.R. Caianaiello", University of Salerno, 84084 Fisciano, Salerno, Italy

* Correspondence: h.beitollahi@kgut.ac.ir (H.B.); adibartolomeo@unisa.it (A.D.B.)

Abstract: We developed a novel hydroxylamine sensor through the surface modification of screen-printed electrode (SPE) with NiCo₂O₄ nanoparticles/reduced graphene oxide (RGO) nanocomposite (NiCo₂O₄/RGO/SPE). We assessed the electrochemical response of hydroxylamine on the as-fabricated sensor, confirming the high electrocatalytic impact of hydroxylamine oxidation. The electrode produced sensitively responded to hydroxylamine under optimized conditions, with a low limit of detection (2.0 nM) and broad linear dynamic range (0.007–385.0 μM). The presence of NiCo₂O₄ combined with the modification of RGO resulted in sensitive detection and signal amplification of hydroxylamine oxidation. The proposed sensor was used to determine the existence of hydroxylamine in water samples.

Keywords: hydroxylamine; NiCo₂O₄/RGO nanocomposite; screen-printed electrode; voltammetry



Citation: Tajik, S.; Beitollahi, H.; Ahmadi, S.a.; Askari, M.B.; Di Bartolomeo, A. Screen-Printed Electrode Surface Modification with NiCo₂O₄/RGO Nanocomposite for Hydroxylamine Detection. *Nanomaterials* **2021**, *11*, 3208. <https://doi.org/10.3390/nano11123208>

Academic Editor: Dong-Joo Kim

Received: 3 November 2021

Accepted: 24 November 2021

Published: 26 November 2021

Publisher's Note: MDPI stays neutral with regard to jurisdictional claims in published maps and institutional affiliations.



Copyright: © 2021 by the authors. Licensee MDPI, Basel, Switzerland. This article is an open access article distributed under the terms and conditions of the Creative Commons Attribution (CC BY) license (<https://creativecommons.org/licenses/by/4.0/>).

1. Introduction

Hydroxylamine, HA or NH₂OH, is an ammonium-containing agent that can act as an intermediate in microbial nitrogen cycle processes, generated during anaerobic ammonium oxidation and nitrification. It has also a function of reducing agent extensively present in various pharmaceutical and industrial applications [1]. Nevertheless, the presence of this agent may show moderate toxicity in humans, plants and animals with reversible and irreversible physiological side effects. The low concentrations (mM) of HA are reportedly found in a stable state for several hours at the pH value of 4.0 but for only 1 h at the pH value of 7.8 in exposure to air [2,3]. Accordingly, it is important to detect HA directly in environmental and biological specimens.

The presence of HA has been recently detected by various techniques, including gas chromatography [4], capillary electrophoresis [5], spectrophotometric [6,7] and chromatography [8,9] analysis, although they involve complex processes. Recently, due to their low cost, operational simplicity, high sensitivity, good selectivity, and fast response, electrochemical techniques have gained attention and have exhibited promising applications for HA analysis [10–15].

Screen-printed electrodes (SPEs) are disposable electrochemical electrodes with advantages like low cost, mass production, disposability and low background current, which can improve multiple shortcomings of carbon paste electrodes and glassy carbon electrodes, such as tedious cleaning procedures and memory impacts. The practical application of

disposable screen-printed electrodes is limited due to shortcomings such as low reproducibility and sensitivity, but their modifiable surface is able to improve various sensing materials in terms of detection performance [16–19]. Hence, the detection of HA can be achieved using the SPEs.

Chemically modified electrodes improve mass transfer kinetics at low overpotential resulting in a decrease the interferences' effect and avoiding surface fouling [20–26]. The performance of the sensors has been improved due to significant advances in nanomaterials, for example in terms of sensitivity and a wide range of detection of target molecules [27–35].

In the structure of the NiCo_2O_4 spinel, the Ni atoms occupy the tetrahedral sites, and the Co atoms occupy the octahedral sites in Co_3O_4 . NiCo_2O_4 , with low activation energy of electron transfer between cations, exhibits better conductivity and electrochemical features compared to pure Co_3O_4 and NiO. Several deficiencies have been reported for NiCo_2O_4 , including low conductivity and easy accumulation on the electrode surface, hence resulting in poor sensitivity [36–38]. We can enhance the electrical conductivity and widen the surface area through the combination of composite materials. Graphene has been recently at the center of attention because of special chemical, optical and electronic properties. In particular, reduced graphene oxide (RGO) has been evaluated and applied in different fields. In electrochemistry, owing to the large surface area, high conductivity and admirable electrochemical responses, RGO has been used to load of other nanomaterials. Composites provide synergistic impacts, which are highly desired in sensor surface modification. The integration of NiCo_2O_4 and graphene can significantly prevent the self-accumulation of individual graphene and metal oxides. The RGO with large surface area and potent electrical conductivity forms further active sites for NiCo_2O_4 , thereby enhancing the sensing potential of NiCo_2O_4 [39–41].

The novelty of this work concerns the observed catalytic action of the $\text{NiCo}_2\text{O}_4/\text{RGO}$ nanocomposite, demonstrating the possibility to detect HA at a low potential and at higher current values. Moreover, the $\text{NiCo}_2\text{O}_4/\text{RGO}/\text{SPE}$ sensor was applied to detect the HA in the different water samples.

2. Materials and Methods

2.1. Chemicals and Equipment

The electrochemical measurements were performed by a PGSTAT 302N Autolab potentiostat/galvanostat analyzer (Eco-Chemie; B.V. Kanaalweg, The Netherlands). All test conditions were monitored by General Purpose Electrochemical System (GPES) software. A three-part DropSens SPE (DRP-110, Asturias, Spain) included a graphite working electrode, a silver pseudo-reference electrode and a graphite auxiliary electrode. The solution pH values were measured by a Metrohm 710 pH meter. Double distilled water was applied to prepare all test fresh solutions. All reagents, including hydroxylamine, possessed analytical grade belonged to Merck (Darmstadt, Germany). Orthophosphoric acid and related salts were utilized to prepare all buffer solutions at the pH values (2.0 to 9.0).

2.2. Fabrication of $\text{NiCo}_2\text{O}_4/\text{RGO}$ Nanocomposite

A modified Hummers method was used to construct the graphene oxide. To this end, the graphite powder (1 g) was first poured into sulfuric acid (200 mL) and stirred for 1 h, followed by placing in the cold-water bath and gradually adding KMnO_4 (9 g) and stirring for 24 h. Then, the obtained mixture was added slowly with deionized water (200 mL) and subsequently with H_2O_2 (35 mL) to stop the oxidation. Next, the product (GO) was exposed to 0.2 M HCl and rinsed by deionized water to discard additional acid.

The NiCo_2O_4 nanorods were produced by dissolving cobalt acetate.4 H_2O (2 mM) and Nickel acetate.4 H_2O (1 mM) in a mixture of deionized water and ethylene glycol (in equal ratios) under the ultrasonication. Then, the mixture was gradually added with polyvinylpyrrolidone (10 mM PVP), stirred for one hour, placed in a Teflon autoclave, and dried in an oven for 16 h at 160 °C. The obtained product was washed by distilled water and ethanol, dried for 24 h at a temperature of 60 °C, and finally calcined at 400 °C for 2 h.

The NiCo₂O₄/RGO was constructed by dissolving GO (100 mg) into a mixture of deionized water and ethylene glycol (with equal ratio), followed by adding the PVP (10 mM) and stirring for 1 h and subsequently adding Co(Ac)₂·4H₂O (2 mM) and Ni(Ac)₂·4H₂O (1 mM) and re-stirring for 2 h. The reaction mixture was placed in the steel autoclave, dried in the oven at 160 °C for 16 h, washed with distilled water-ethanol mix, re-dried at 60 °C for 24 h, and finally calcined at 400 °C for 2 h to collect spinel NiCo₂O₄/RGO. The RGO:NiCo₂O₄ weight ratio was approximately 1:2.

2.3. Fabrication of Modified Electrode

A facile protocol was performed to cover the bare SPE using the NiCo₂O₄/RGO nanocomposite. Thus, 1 mg of NiCo₂O₄/RGO nanocomposite was dispersed in 1 mL aqueous solution and ultra-sonicated for half an hour to give a homogeneous solution. Then, 4 µL of prepared suspension was dropped on the surface of SPE surface. After the solvent evaporated, the electrode surface was thoroughly rinsed with deionized water to wash away the unremoved modifier and dried at room temperature. The obtained electrode was noted as NiCo₂O₄/RGO/SPE.

In order to investigate the available active surface area of electrodes, the cyclic voltammograms bare SPE and NiCo₂O₄/RGO/SPE were recorded in 1 mM K₃Fe(CN)₆ at different scan rates. Using the Randles–Sevcik equation [42], the electrochemical active surface area of NiCo₂O₄/RGO/SPE was found 0.01 cm² which was about 3.2 times greater than bare SPGE.

2.4. Real Sample Analysis

The real specimens included river, drinking and tap water samples, which were filtered thoroughly before analysis and then different amounts of HA concentrations were added to the samples and analyzed using standard addition method.

3. Results

3.1. Determination of the NiCo₂O₄/RGO Nanocomposite Characteristics

The XRD method was used to evaluate NiCo₂O₄/RGO and NiCo₂O₄ for crystal structure. Figure 1 shows the 2θ angles of XRD peaks and corresponding planes, in line with the previous findings and JCPDS (20-078).

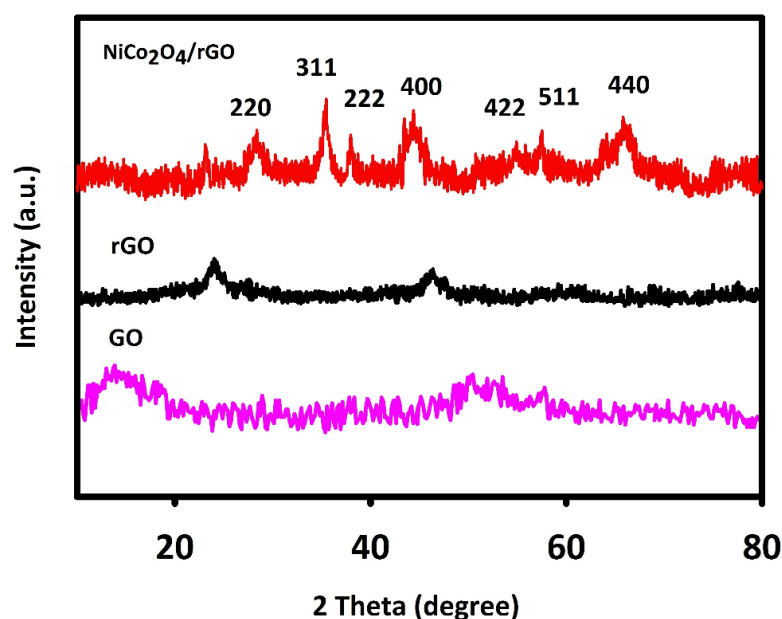


Figure 1. X-ray diffraction (XRD) spectra recorded for fabricated graphene oxide (GO), reduced GO (RGO) and NiCo₂O₄/RGO.

The 2θ values of 64.86° , 59.16° , 55.28° , 44.54° , 38.48° , 36.61° and 31.09° were related to the cubic NiCo_2O_4 phase planes of (440), (511), (422), (400), (222), (311) and (220) in line with JCPDS [20-0781] and previous findings. The wide peak ($2\theta = 25^\circ$) corresponded to RGO. GO has a relatively wide characteristic peak at 2θ about 10° , which indicates the graphite was fully oxidized into GO. The mean crystallite size of $\text{NiCo}_2\text{O}_4/\text{RGO}$ was calculated to be 70 nm in accordance with the Debye–Scherrer equation.

The Raman spectra recorded for fabricated materials are shown in Figure 2. The wide peaks at 1583 and 1330 cm^{-1} were related to $\text{NiCo}_2\text{O}_4/\text{RGO}$ and RGO, corresponding to G and D bands, respectively. The peak of Raman G band was related to in-plane movement of sp^2 carbons, and the Raman D band peak to sp^3 (out-of-plane vibrations).

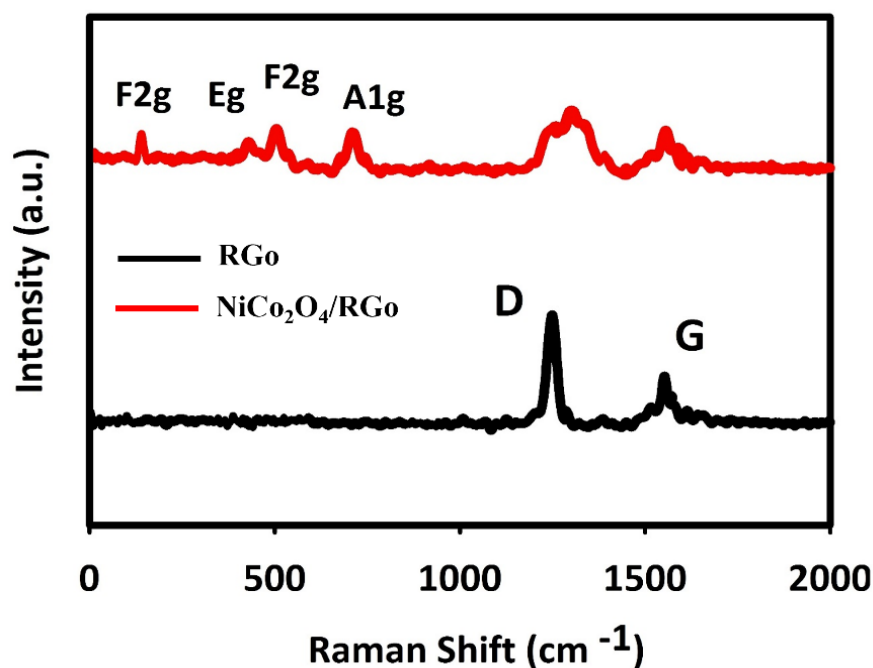


Figure 2. Raman spectra recorded for $\text{NiCo}_2\text{O}_4/\text{RGO}$ and RGO.

The D/G ratio is higher in the composite RGO than in the pure RGO. The elevated D/G ratio means the RGO hybridization with NiCo_2O_4 , enhancing the defect density in RGO and defect in carbon layers. The peaks of Ni–O and Co–O vibrations at 654 , 501 , 456 and 181 cm^{-1} were, respectively, related to A1g, F2g, Eg and F2g of phonon types of NiCo_2O_4 .

To study the surface morphology and also to prove the presence of hybrid constituent elements, scanning electron microscope (SEM) images and energy-dispersive X-ray analysis (EDX) mapping were prepared. Figure 3a shows NiCo_2O_4 nanoparticles. The average size of these nanorods is about 40 nm, and in this figure, a uniform rod-shaped morphology can be seen. RGO nanosheets are also shown in Figure 3b. The plate morphology of these two-dimensional materials is also clearly shown in this image. In the case of hybrids used in electrochemical processes, one of the most important parameters is the uniform dispersion of nanomaterials on a substrate. Figure 3c clearly shows the uniform distribution of NiCo_2O_4 nanorods on the surface of RGO. The presence of nano-hybrid constituents, including nickel, cobalt, oxygen, and carbon was confirmed by the EDX mapping analysis (Figure 3d).

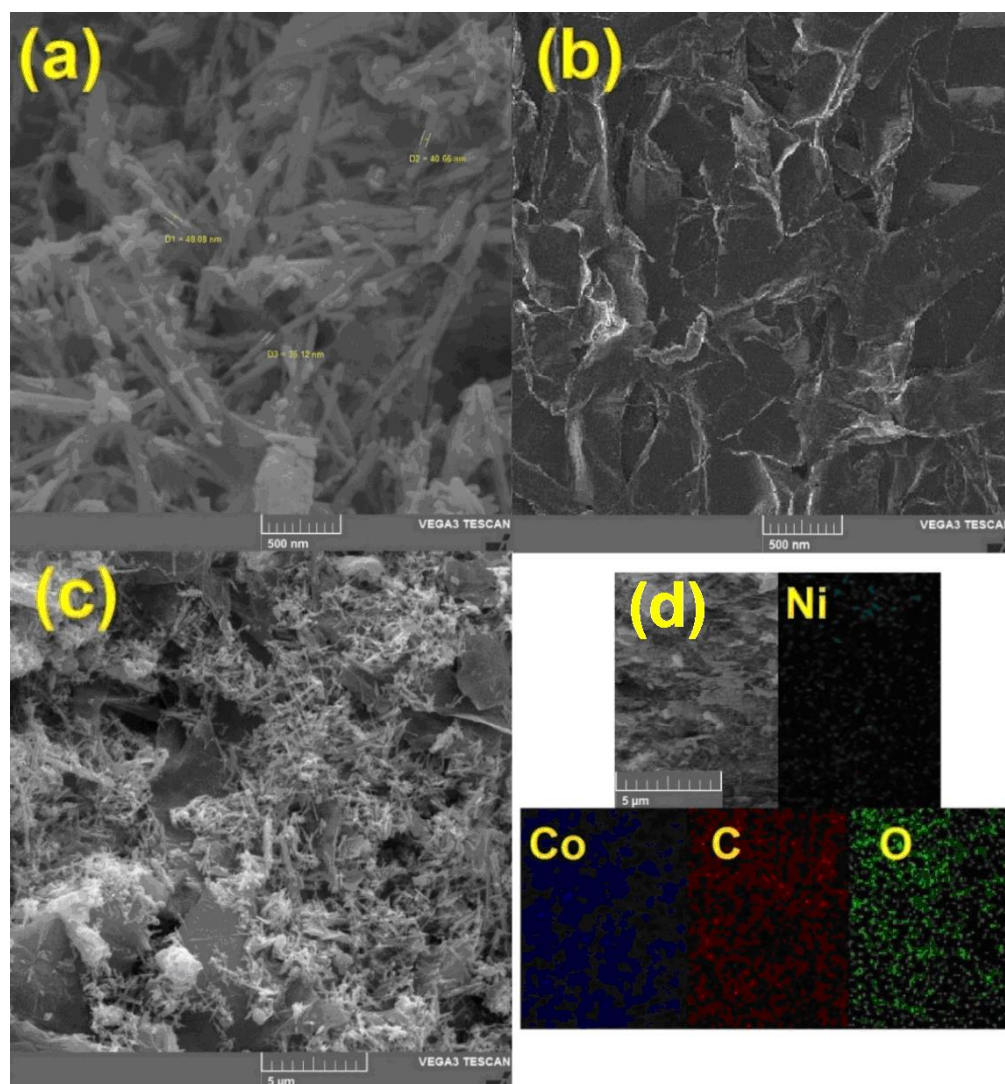


Figure 3. The scanning electron microscopy (SEM) images taken from (a) NiCo_2O_4 nanorod, (b) RGO nanosheets, (c) $\text{NiCo}_2\text{O}_4/\text{RGO}$ and (d) The energy-dispersive X-ray analysis (EDX) mapping of $\text{NiCo}_2\text{O}_4/\text{RGO}$.

3.2. Electrochemical Responses of Hydroxylamine on the Surface of $\text{NiCo}_2\text{O}_4/\text{Reduced Graphene Oxide (RGO)/Screen-Printed Electrode (SPE)}$

The solution pH values influence the electrochemical responses of HA, highlighting the necessity for optimizing the solution pH to determine the electrocatalytic HA oxidation, which was evaluated in 0.1 M PBS at various pH values (2.0 to 9.0) on the $\text{NiCo}_2\text{O}_4/\text{RGO}/\text{SPE}$ surface using cyclic voltammetry. The results suggested neutral pH value to achieve the best outcomes of HA electrooxidation on the $\text{NiCo}_2\text{O}_4/\text{RGO}/\text{SPE}$ surface. Hence, the optimal pH value was selected to be 7.0 for this purpose in the next testing.

Figure 4 (curves a and b) shows the cyclic voltammograms (CVs) recorded for electrooxidation of HA (100.0 μM) on the surfaces of bare SPE and $\text{NiCo}_2\text{O}_4/\text{RGO}/\text{SPE}$. The findings from the CVs confirmed the best HA oxidation on the $\text{NiCo}_2\text{O}_4/\text{RGO}/\text{SPE}$ surface at 750 mV, about 250 mV more negative than that on the bare SPE, underlining a significant improvement of HA oxidation signal via the $\text{NiCo}_2\text{O}_4/\text{RGO}$ nanocomposite.

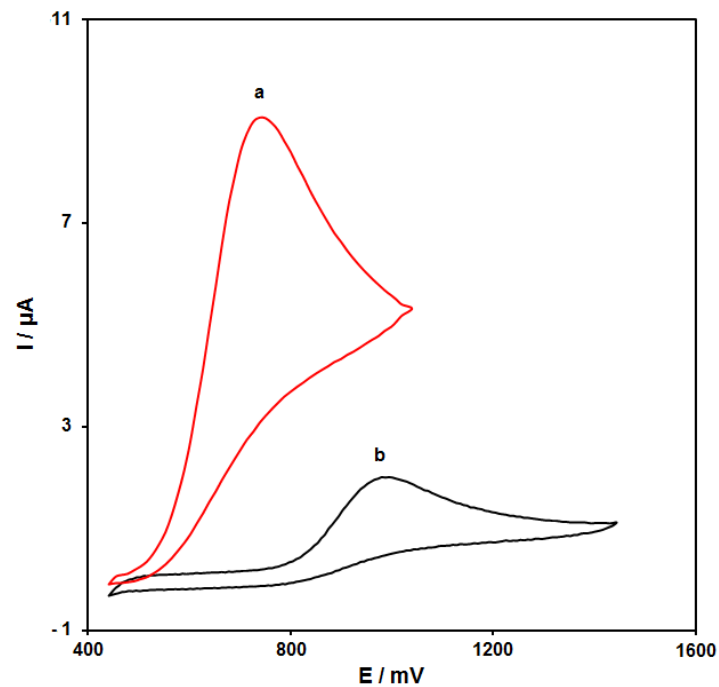


Figure 4. Cyclic voltammograms (CVs) of bare screen-printed electrode (SPE) (a) and NiCo₂O₄/RGO/SPE (b) in the presence of 0.1 M phosphate-buffered saline (PBS) at the pH value of 7.0 for detection of HA (100.0 μM) at the scan rate of 50 mV/s.

3.3. Results of Scan Rate Impact

Figure 5 shows the scan rate impact on the HA oxidation current, the results of which indicated an increase in the peak current with increasing scan rate. The oxidation process followed the diffusion-limited reactions obtained from the linear dependence of the anodic peak current (I_p) on the square root of the scan rate ($v^{1/2}$, 10–400 mV/s).

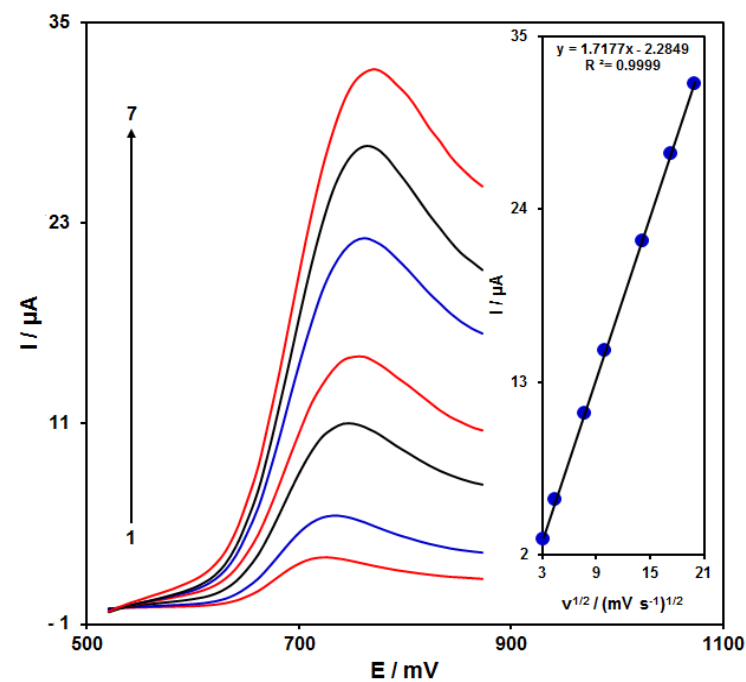


Figure 5. LSVs of NiCo₂O₄/RGO/SPE in the presence of 0.1 M PBS at the pH value of 7.0 for detection of HA (150.0 μM) at different scan rates, indicating numbers 1–7 as 10, 20, 60, 100, 200, 300 and 400 mV/s. Inset: anodic peak current variation versus $v^{1/2}$.

3.4. Chronoamperometric Measurements

Chronoamperometry was employed to evaluate the catalytic HA oxidation on the modified electrode surface in the presence of different HA concentrations on the working electrode set at the potential value of 800 mV. The HA diffusion coefficient was also determined. According to previous findings, the electrochemical current of HA under the mass transport-limited condition could be calculated using the Cottrell method:

$$I = nFAD^{1/2} C_b \pi^{-1/2} t^{-1/2}$$

In this equation, D and C_b stand for diffusion coefficient (cm^2/s) and bulk concentration (mol/cm^3), respectively. Figure 6A shows the plot of I versus $t^{-1/2}$ on the basis of experiments for various HA specimens. Figure 6B displays the slope of straight line versus HA content. The D value for HA was calculated to be $2.2 \times 10^{-5} \text{ cm}^2/\text{s}$ based on the Cottrell equation and the slopes obtained.

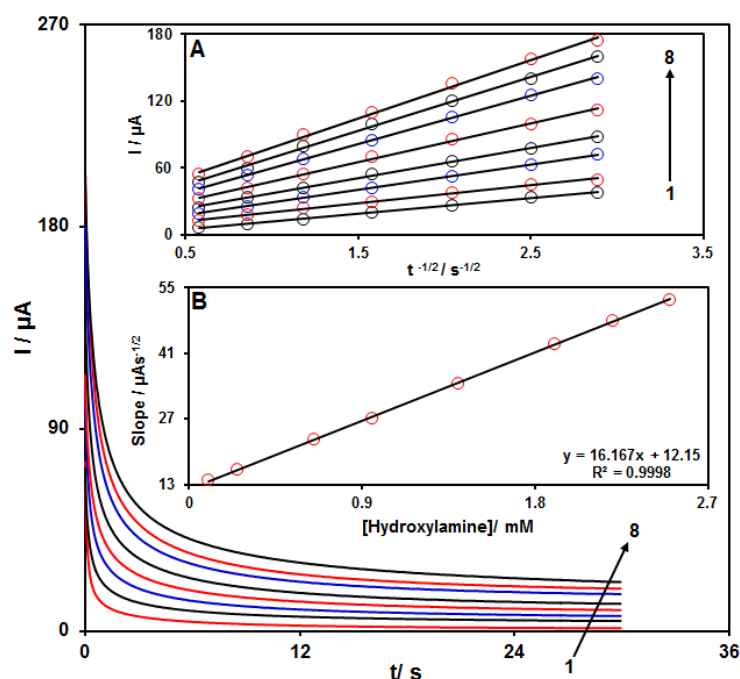


Figure 6. Chronoamperograms for $\text{NiCo}_2\text{O}_4/\text{RGO}/\text{SPE}$ in the presence of 0.1 M PBS at the pH value of 7.0 for detection of HA at different concentrations, indicating numbers 1–8 as 0.1, 0.25, 0.65, 0.95, 1.4, 1.9, 2.2 and 2.5 mM of HA. Insets: (A) Cottrell plot for chronoamperogram findings, (B) slope of the plot of straight lines versus HA content.

3.5. Calibration Curve and Limit of Detection

The peak currents of HA electro-oxidation on the $\text{NiCo}_2\text{O}_4/\text{RGO}/\text{SPE}$ surface were used for the HA detection. Because hypersensitivity and appropriate analytical features are the advantages of differential pulse voltammetry (DPV), different HA concentrations in the $\text{NiCo}_2\text{O}_4/\text{RGO}/\text{SPE}$ and PBS (0.1 M) were used for DPV analysis as shown in Figure 7 (response time = 6 s). The peak currents of HA oxidation on the surface of $\text{NiCo}_2\text{O}_4/\text{RGO}/\text{SPE}$ depends linearly on HA concentrations (0.007 to 385.0 μM). The linear equation was as $y = 0.0805x + 0.9398$, the correlation coefficient was estimated at 0.9999, but the limit of detection (3σ) was estimated at 2.0 nM. The LOD and linear range of HA at the $\text{NiCo}_2\text{O}_4/\text{RGO}/\text{SPE}$ electrode presented in this work were compared with the reported modified electrodes and were given in Table 1.

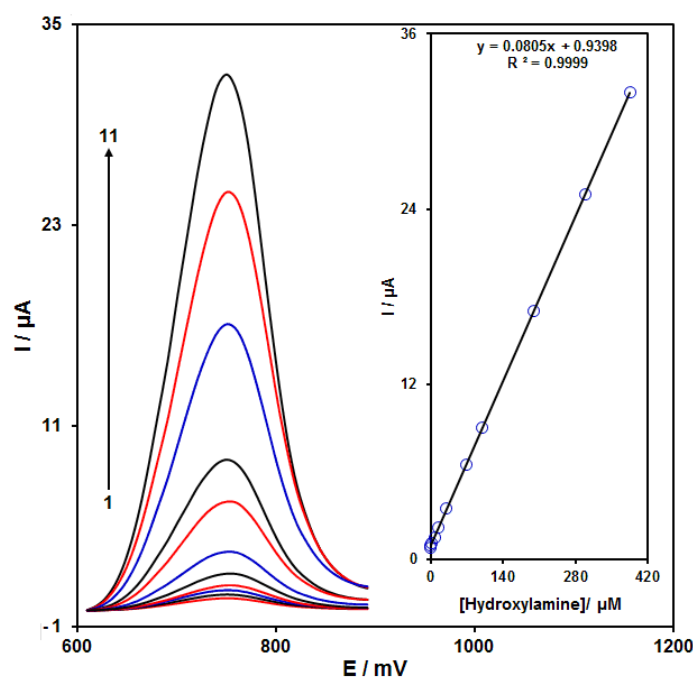


Figure 7. DPVs of NiCo₂O₄/RGO/SPE in the presence of 0.1 M PBS at the pH value of 7.0 for detection of hydroxylamine (HA) at different concentrations, indicating numbers 1–11 as 0.007, 0.1, 1.0, 7.5, 15.0, 30.0, 70.0, 100.0, 200.0, 300.0 and 385.0 μM of HA. Inset: plot of peak current as a function of different HA concentrations (0.007–385.0 μM).

Table 1. Comparison of the efficiency of the NiCo₂O₄/RGO/SPE electrode with literature modified electrodes for HA determination.

Electrochemical Sensor	Electrochemical Method	Linear Range	Limit of Detection	Ref.
Fullerene-functionalized carbon nanotubes/ionic liquid nanocomposite/glassy carbon electrode	DPV	1.0–300.0 μM	28 ± 2 nM	[10]
Graphene oxide/TiO ₂ /SPE	DPV	0.1–300 μM	0.065 μM	[11]
Gold nanoparticles/cetyltrimethyl ammonium bromide/graphene oxide/glassy carbon electrode	Amperometry	10–1000 μM	3.5 μM	[12]
Prussian blue-multi-walled carbon nanotubes/glassy carbon electrode	Amperometry	1.5 μM –2.0 mM	-	[13]
Gold nanoparticles—polypyrrole nanowire/glassy carbon electrode	DPV	1–500 μM	0.21 μM	[14]
1-benzyl-4-ferrocenyl-1H-[1-3]-triazole/carbon nanotube/glassy carbon electrode	Square wave voltammetry	4.0×10^{-7} – 6.75×10^{-4} M	28.0 ± 1.0 nM	[15]
NiCo ₂ O ₄ /RGO/SPE	DPV	0.007–385.0 μM	2.0 nM	This Work

3.6. Interference Study

The impact of numerous interference substances on the detection of HA was investigated. The tolerance limit was taken as the maximum of the foreign materials concentration that resulted in about $\pm 5\%$ relative error in the detection. The results indicated that glucose, lactose, sucrose, urea, sulfite, hydrazine, phenol, thiosulphate, bisphenol A, Mg²⁺, Ni²⁺, K⁺, Li⁺, Mn²⁺, Cr²⁺, Zn²⁺, CN⁻, Br⁻, and SCN⁻ did not show interference in the determination of HA.

3.7. Real Sample Analysis

The fabricated NiCo₂O₄/RGO/SPE was used for the detection of HA present in varied water specimens using the method of standard additions. The HA concentration and recovery rate are shown in Table 2. An excellent recovery rate was found for the HA, and mean relative standard deviation (RSD%) confirmed the reproducibility. The applicability of NiCo₂O₄/RGO/SPE sensor was confirmed by sensitive detection of HA concentrations in drinking, tap and river water specimens.

Table 2. Recoveries for detection of hydroxylamine in water specimens ($n = 5$).

Sample	Spiked	Found	Recovery (%)	R.S.D. (%)
Drinking water	0	-	-	-
	5.0	4.9	98.0	3.2
	7.0	7.3	104.3	2.7
	9.0	9.1	101.1	1.9
	11.0	10.9	99.1	2.4
Tap water	0	-	-	-
	4.5	4.6	102.2	2.9
	6.5	6.3	97.0	3.5
	8.5	8.4	98.8	1.6
	10.5	10.6	100.9	2.5
River water	0	-	-	-
	5.5	5.4	98.2	2.7
	7.5	7.8	104.0	2.1
	9.5	9.6	101.0	3.6
	11.5	11.4	99.1	2.0

4. Conclusions

In this work, we prepared NiCo₂O₄/RGO nanocomposite by a simple method. The successful preparation of this nanocomposite was revealed by FESEM, EDX mapping, XRD, and Raman spectroscopy. Then, we developed a novel voltammetric hydroxylamine sensor through the surface modification of SPE with NiCo₂O₄/RGO nanocomposite as a signal amplifier for HA detection. The oxidation peak currents of HA presented a good linear relationship with the concentrations in the range from 0.007 to 385.0 μ M with a detection limit of 2.0 nM. Moreover, the detection of HA in water samples by the proposed sensor showed satisfactory results.

Author Contributions: Conceptualization, H.B. and A.D.B.; methodology, S.a.A. and M.B.A.; software, S.T., S.a.A. and M.B.A.; validation, S.T., A.D.B. and H.B.; formal analysis, S.T., S.a.A. and M.B.A.; investigation, S.T., S.a.A., M.B.A.; resources, H.B. and A.D.B.; data curation, H.B., S.a.A. and A.D.B.; writing—original draft preparation, S.T. and H.B.; writing—review and editing, A.D.B.; visualization, S.T., S.a.A. and M.B.A.; supervision, H.B. and A.D.B.; project administration, H.B. and A.D.B.; funding acquisition, H.B. and A.D.B. All authors have read and agreed to the published version of the manuscript.

Funding: This research was funded by University of Salerno, grant number ORSA218189 and ORSA200207.

Data Availability Statement: The data presented in this study are available on request from the corresponding author.

Conflicts of Interest: The authors declare no conflict of interest.

References

1. Fernando, P.N.; Egwu, I.N.; Hussain, M.S. Ion chromatographic determination of trace hydroxylamine in waste streams generated by a pharmaceutical reaction process. *J. Chromatogr. A* **2002**, *956*, 261–270. [[CrossRef](#)]
2. Fiadeiro, M.; Solorzano, L.; Strickland, J.D.H. Hydroxylamine in sea water. *Limnol. Oceanogr.* **1967**, *12*, 555–556. [[CrossRef](#)]
3. Anderson, J.H. The copper-catalysed oxidation of hydroxylamine. *Analyst* **1964**, *89*, 357–362. [[CrossRef](#)]

4. Seike, Y.; Fukumori, R.; Senga, Y.; Oka, H.; Fujinaga, K.; Okumura, M. A simple and sensitive method for the determination of hydroxylamine in fresh-water samples using hypochlorite followed by gas chromatography. *Anal. Sci.* **2004**, *20*, 139–142. [[CrossRef](#)]
5. You, T.; Wu, M.; Wang, E. Determination of hydroxylamine by capillary electrophoresis-electrochemical detection with a palladium-particle modified carbon fiber microdisk array electrode. *Anal. Lett.* **1997**, *30*, 1025–1036. [[CrossRef](#)]
6. Frear, D.S.; Burrell, R.C. Spectrophotometric method for determining hydroxylamine reductase activity in higher plants. *Anal. Chem.* **1955**, *27*, 1664–1665. [[CrossRef](#)]
7. Hu, B.; Tian, X.L.; Shi, W.N.; Zhao, J.Q.; Wu, P.; Mei, S.T. Spectrophotometric determination of hydroxylamine in biological wastewater treatment processes. *Int. J. Environ. Sci. Technol.* **2018**, *15*, 323–332. [[CrossRef](#)]
8. Bezy, V.; Morin, P.; Couerbe, P.; Leleu, G.; Agrofoglio, L. Simultaneous analysis of several antiretroviral nucleosides in rat-plasma by high-performance liquid chromatography with UV using acetic acid/hydroxylamine buffer: Test of this new volatile medium-pH for HPLC–ESI-MS/MS. *J. Chromatogr. B* **2005**, *821*, 132–143. [[CrossRef](#)]
9. Li, N.; Deng, C.; Yao, N.; Shen, X.; Zhang, X. Determination of acetone, hexanal and heptanal in blood samples by derivatization with pentafluorobenzyl hydroxylamine followed by headspace single-drop microextraction and gas chromatography–mass spectrometry. *Anal. Chim. Acta* **2005**, *540*, 317–323. [[CrossRef](#)]
10. Mazloun-Ardakani, M.; Khoshroo, A.; Hosseinzadeh, L. Simultaneous determination of hydrazine and hydroxylamine based on fullerene-functionalized carbon nanotubes/ionic liquid nanocomposite. *Sens. Actuators B Chem.* **2015**, *214*, 132–137. [[CrossRef](#)]
11. Malakooti, M.; Gholami, Z.; Mahmoudi-Moghaddam, H. Electrochemical determination of hydroxylamine in water samples using modified screen-printed electrode with TiO₂/GO. *Int. J. Environ. Anal. Chem.* **2021**, *101*, 35–47. [[CrossRef](#)]
12. Yang, Y.J.; Li, W. Gold nanoparticles/graphene oxide composite for electrochemical sensing of hydroxylamine and hydrogen peroxide. *Fuller. Nanotub. Carbon Nanostruct.* **2018**, *26*, 195–204. [[CrossRef](#)]
13. Zhang, N.; Wang, G.; Gu, A.; Feng, Y.; Fang, B. Fabrication of prussian blue/multi-walled carbon nanotubes modified electrode for electrochemical sensing of hydroxylamine. *Microchim. Acta* **2010**, *168*, 129–134. [[CrossRef](#)]
14. Li, J.; Lin, X. Electrocatalytic oxidation of hydrazine and hydroxylamine at gold nanoparticle—polypyrrole nanowire modified glassy carbon electrode. *Sens. Actuators B Chem.* **2007**, *126*, 527–535. [[CrossRef](#)]
15. Beitollahi, H.; Tajik, S.; Mohammadi, S.Z.; Baghayeri, M. Voltammetric determination of hydroxylamine in water samples using a 1-benzyl-4-ferrocenyl-1H-[1, 2, 3]-triazole/carbon nanotube-modified glassy carbon electrode. *Ionics* **2014**, *20*, 571–579. [[CrossRef](#)]
16. Tajik, S.; Beitollahi, H.; Won Jang, H.; Shokouhimehr, M. A screen printed electrode modified with Fe₃O₄@polypyrrole-Pt core-shell nanoparticles for electrochemical detection of 6-mercaptopurine and 6-thioguanine. *Talanta* **2021**, *232*, 122379. [[CrossRef](#)]
17. Altun, M.; Bilgi Kamaç, M.; Bilgi, A.; Yilmaz, M. Dopamine biosensor based on screen-printed electrode modified with reduced graphene oxide, polynuclear red and gold nanoparticle. *Int. J. Environ. Anal. Chem.* **2020**, *100*, 451–467. [[CrossRef](#)]
18. Garkani Nejad, F.; Beitollahi, H.; Tajik, S.; Jahani, S. La³⁺-doped Co₃O₄ nanoflowers modified graphite screen printed electrode for electrochemical sensing of vitamin B₆. *Anal. Bioanal. Chem. Res.* **2019**, *6*, 69–79.
19. Tajik, S.; Beitollahi, H.; Shahsavari, S.; Garkani Nejad, F. Simultaneous and selective electrochemical sensing of methotrexate and folic acid in biological fluids and pharmaceutical samples using Fe₃O₄/ppy/Pd nanocomposite modified screen printed graphite electrode. *Chemosphere* **2021**. [[CrossRef](#)]
20. Karimi-Maleh, H.; Sheikhsheoie, M.; Sheikhsheoie, I.; Ranjbar, M.; Alizadeh, J.; Maxakato, N.W.; Abbaspourrad, A. A novel electrochemical epinine sensor using amplified CuO nanoparticles and an-hexyl-3-methylimidazolium hexafluorophosphate electrode. *New J. Chem.* **2019**, *43*, 2362–2367. [[CrossRef](#)]
21. Ganjali, M.R.; Garkani-Nejad, F.; Tajik, S.; Beitollahi, H.; Pourbasheer, E.; Larijani, B. Determination of salicylic acid by differential pulse voltammetry using ZnO/Al₂O₃ nanocomposite modified graphite screen printed electrode. *Int. J. Electrochem. Sci.* **2017**, *12*, 9972–9982. [[CrossRef](#)]
22. Karimi-Maleh, H.; Tahernejad-Javazmi, F.; Ensafi, A.A.; Moradi, R.; Mallakpour, S.; Beitollahi, H. A high sensitive biosensor based on FePt/CNTs nanocomposite/N-(4-hydroxyphenyl)-3,5-dinitrobenzamide modified carbon paste electrode for simultaneous determination of glutathione and piroxicam. *Biosens. Bioelectron.* **2014**, *60*, 1–7. [[CrossRef](#)] [[PubMed](#)]
23. Beitollahi, H.; Tajik, S.; Garkani-Nejad, F.; Safaei, M. Recent advances in ZnO nanostructure-based electrochemical sensors and biosensors. *J. Mater. Chem. B* **2020**, *8*, 5826–5844. [[CrossRef](#)]
24. Prasad, P.; Sreedhar, N.Y. Effective SWCNTs/Nafion electrochemical sensor for detection of dicapthon pesticide in water and agricultural food samples. *Chem. Methodol.* **2018**, *2*, 277–290.
25. Baghizadeh, A.; Karimi-Maleh, H.; Khoshnama, Z.; Hassankhani, A.; Abbasghorbani, M. A voltammetric sensor for simultaneous determination of vitamin C and vitamin B₆ in food samples using ZrO₂ nanoparticle/ionic liquids carbon paste electrode. *Food Anal. Methods* **2015**, *8*, 549–557. [[CrossRef](#)]
26. Mahalakshmi, S.; Sridevi, V. In situ electrodeposited gold nanoparticles on polyaniline-modified electrode surface for the detection of dopamine in presence of ascorbic acid and uric acid. *Electrocatalysis* **2021**, *12*, 415–435. [[CrossRef](#)]
27. Tajik, S.; Beitollahi, H.; Garkani Nejad, F.; Safaei, M.; Mohammadzadeh Jahani, P. Electrochemical sensing of Sudan I using the modified graphite screen-printed electrode. *Int. J. Environ. Anal. Chem.* **2020**. [[CrossRef](#)]
28. Karimi-Maleh, H.; Karimi, F.; Fu, L.; Sanati, A.L.; Alizadeh, M.; Karaman, C.; Orooji, Y. Cyanazine herbicide monitoring as a hazardous substance by a DNA nanostructure biosensor. *J. Hazard. Mater.* **2022**, *423*, 127058. [[CrossRef](#)]

29. Hosseini Fakhrabad, A.; Sanavi Khoshnood, R.; Abedi, M.R.; Ebrahimi, M. Fabrication a composite carbon paste electrodes (CPEs) modified with Multi-Wall Carbon Nano-Tubes (MWCNTs/N, N-Bis(salicyliden)-1,3-propandiamine) for determination of lanthanum (III). *Eurasian Chem. Commun.* **2021**, *3*, 627–634.
30. Bodur, O.C.; Dinç, S.; Özmen, M.; Arslan, F. A sensitive amperometric detection of neurotransmitter acetylcholine using carbon dot-modified carbon paste electrode. *Biotechnol. Appl. Biochem.* **2021**, *68*, 20–29. [[CrossRef](#)]
31. Karimi-Maleh, H.; Alizadeh, M.; Orooji, Y.; Karimi, F.; Baghayeri, M.; Rouhi, J.; Tajik, S.; Beitollahi, H.; Agarwal, S.; Gupta, V.K. Guanine-based DNA biosensor amplified with Pt/SWCNTs nanocomposite as analytical tool for nanomolar determination of daunorubicin as an anticancer drug: A docking/experimental investigation. *J. Ind. Eng. Chem.* **2021**, *60*, 816–823. [[CrossRef](#)]
32. Tajik, S.; Beitollahi, H.; Garkani Nejad, F.; Sheikhshoaie, I.; Nugraha, A.S.; Jang, H.W.; Yamauchi, Y.; Shokouhimehr, M. Performance of metal–organic frameworks in the electrochemical sensing of environmental pollutants. *J. Mater. Chem. A* **2021**, *9*, 8195–8220. [[CrossRef](#)]
33. Song, P.; Li, Y.; Yin, S.; Tang, Y.; Wang, Z. Simulation-based evaluation of homogeneous electrocatalytic reaction within a thin layer modified electrode. *J. Electroanal. Chem.* **2021**, *901*, 115784. [[CrossRef](#)]
34. Mehri-Talarposhti, F.; Ghorbani-Hasan Saraei, A.; Golestan, L.; Shahidi, S.A. Electrochemical determination of Vitamin B₆ in fruit juices using a new nanostructure voltammetric sensor. *Asian J. Nanosci. Mater.* **2020**, *3*, 313–320.
35. Hu, W.C.; Pang, J.; Biswas, S.; Wang, K.; Wang, C.; Xia, X.H. Ultrasensitive detection of bacteria using a 2D MOF nanozyme-amplified electrochemical detector. *Anal. Chem.* **2021**, *93*, 8544–8552. [[CrossRef](#)]
36. Zhang, G.; Xia, B.Y.; Wang, X.; Lou, X.W. Strongly coupled NiCo₂O₄-rGO hybrid nanosheets as a methanol-tolerant electrocatalyst for the oxygen reduction reaction. *Adv. Mater.* **2014**, *26*, 2408–2412. [[CrossRef](#)] [[PubMed](#)]
37. Xue, S.; Wang, K.; Cheng, Y.; Tu, B.; Xia, Y.; Yuan, S.; Tao, H. Simultaneous determination of catechol and hydroquinone with L-cysteine and nickel cobaltite Co-functionalised graphene oxide modified glassy carbon electrode. *Int. J. Environ. Anal. Chem.* **2021**. [[CrossRef](#)]
38. Zhao, H.; Xu, J.; Sheng, Q.; Zheng, J.; Cao, W.; Yue, T. NiCo₂O₄ nanorods decorated MoS₂ nanosheets synthesized from deep eutectic solvents and their application for electrochemical sensing of glucose in red wine and honey. *J. Electrochem. Soc.* **2019**, *166*, H404. [[CrossRef](#)]
39. Osaimany, P.; Samuel, A.S.; Johnbosco, Y.; Kharwar, Y.P.; Chakravarthy, V. A study of synergistic effect on oxygen reduction activity and capacitive performance of NiCo₂O₄/rGO hybrid catalyst for rechargeable metal-air batteries and supercapacitor applications. *Compos. Part B Eng.* **2019**, *176*, 107327. [[CrossRef](#)]
40. Lv, A.; Lu, S.; Xu, W.; Wang, Z.; Shen, Y.; Liu, G. One-pot synthesis of NiCo₂O₄/rGO/NF hybrid electrode materials realizing ultrahigh capacitance and rapid charge/discharge at large current density. *Appl. Surf. Sci.* **2020**, *511*, 145538. [[CrossRef](#)]
41. Wang, B.; Cao, Y.; Chen, Y.; Lai, X.; Peng, J.; Tu, J.; Li, X. Rapid synthesis of rGO conjugated hierarchical NiCo₂O₄ hollow mesoporous nanospheres with enhanced glucose sensitivity. *Nanotechnology* **2016**, *28*, 025501. [[CrossRef](#)] [[PubMed](#)]
42. Bard, A.J.; Faulkner, L.R. *Electrochemical Methods: Fundamentals and Applications*, 2nd ed.; John Wiley & Sons: New York, NY, USA, 2001.